

Multifrequency study of a double–double radio galaxy J1706+4340

A. Marecki¹★, M. Jamrozy², J. Machalski²

¹*Toruń Centre for Astronomy, Faculty of Physics, Astronomy and Informatics, Nicolaus Copernicus University, Grudziądzka 5, PL-87-100 Toruń, Poland*

²*Astronomical Observatory, Jagiellonian University, ul. Orla 171, PL-30-244 Kraków, Poland*

Accepted 2016 August 8. Received 2016 August 5; in original form 2016 June 20

ABSTRACT

We report the outcome of multifrequency radio observations of a double–double radio source J1706+4340 carried out with the Very Large Array and Giant Metrewave Radio Telescope. After supplementing our own data with those available in the literature, we collected a considerable set of radio measurements covering the range from 74 to 8460 MHz. This has enabled us to perform a comprehensive review of physical properties of the source and its dynamical evolution analysis. In particular, we found that, while the age of the large-scale outer lobes is in the range 260–300 Myr, the renewal of the jet activity, which is directly responsible for the double–double structure, took place only about 12 Myr ago after about 27-Myr long period of quiescence. Another important property of J1706+4340 we found is that the injection spectral indices and the jet powers for the inner and the outer doubles are very similar. This implies that it is the spin of the supermassive black hole rather than e.g. an instability of the accretion disc that is likely responsible for the jet production and its properties.

Key words:

radiation mechanisms: non-thermal – galaxies: individual: J1706+4340 – galaxies: jets – radio continuum: galaxies

1 INTRODUCTION

Lobes of radio sources associated with active galactic nuclei (AGNs) are huge reservoirs of energy so even when fuelling provided by the jets is cut-off, they are still observable, albeit in a relic form, for a substantial amount of time. Komissarov & Gubanov (1994) argue that the so-called coasting phase of the lobes may last up to 10^8 yr hence it is quite likely that ignition of a new active episode can still take place during the coasting phase, i.e. before the lobes have faded completely. The observable effect of this coincidence would be the presence of a new pair of radio lobes straddled with an old, larger, double-lobed relic structure. If both pairs of lobes are co-linear and if there is a common centre of symmetry located at the galactic nucleus then the whole such structure is labelled a double–double radio source (DDRS). The list of best-known DDRSs and the review of their properties has been given by Saikia & Jamrozy (2009).

Since the outer lobes of DDRSs are no longer fuelled, they have steep spectra due to ageing, thus they are best observable at low radio frequencies. To attain high resolution at that part of the spectrum, numerous DDRSs have been targeted by Giant Metrewave Radio Telescope (GMRT). Nevertheless, the most comprehensive approach in such investigations is to combine the GMRT low-frequency data with the Very Large Array (VLA) data obtained at higher frequencies. To date, only few

DDRSs, e.g. J1453+3308 (Konar et al. 2006) and PKS 1545–321 (Machalski, Jamrozy & Konar 2010), have been investigated this way. Owing to determination of their spectra over a wide frequency range, many of the astrophysical parameters could be established, including the ages of both inner and outer lobes as well as the length of the quiescence period between two epochs of activity the two pairs of lobes are signatures of.

In this article, radio data for J1706+4340 gathered in the range from 74 to 8460 MHz, predominantly by means of the GMRT and VLA observations, are analysed in order to study the dynamics and energetics of this source. The paper is organized as follows. The discovery of the J1706+4340 as a DDRS is introduced in Section 2, optical and infrared data of the host galaxy are quoted in Section 3, and multifrequency radio data are presented in Section 4. The dynamical analysis of each pair of radio lobes of J1706+4340 is elaborated upon in Section 5. The results are discussed in Section 6 and summarized in Section 7.

The cosmological parameters by (Spergel et al. 2003, $H_0 = 71 \text{ km s}^{-1} \text{ Mpc}^{-1}$, $\Omega_M = 0.27$, and $\Omega_\Lambda = 0.73$) are used throughout this article. Positions are given in the J2000.0 coordinate system.

2 THE DOUBLE–DOUBLE NATURE OF J1706+4340

J1706+4340 (B3 1704+437) has not been studied in detail to date although its double–double nature has been recognized. Proctor (2011) listed J1706+4340 as one of 242 double–doubles iden-

★ E-mail: amr@astro.uni.torun.pl

Table 1. Radio data of J1706+4340 analysed in this study

Frequency (MHz)	Telescope/ Survey	Date of observation	Beam size and PA			rms (mJy beam ⁻¹)	Ref.
(1)	(2)	(3)	(4)			(5)	(6)
73.8	VLA-B/VLSSr	2003 Sep 20	75	75		180.7	1
151.5	Cambridge/6C	1976–1978	252.0	364.9		40	2
152.2	GMRT	2011 Aug 25	24.78	21.33	−36.60	5.19	p
232.0	MSRT	1985–1993	228.0	330.2		50.0	3
240.1	GMRT	2011 Aug 31	36.85	10.63	−69.20	2.92	p
326.9	WSRT/WENSS	1991	54	78.2		3.25	4
408.0	Northern Cross/B3	1977 Feb–May	156	288.96		10	5
612.2	GMRT	2011 Aug 31	5.82	4.82	−3.36	0.071	p
1400.0	VLA-D/NVSS	1995 Mar 12	45	45		0.45	6
1400.0	VLA-B/FIRST	1994 Aug 19	5.4	5.4		0.18	7
1425.0	VLA-A	2006 Feb 21	1.35	1.06	29.99	0.0764	p
1425.0	VLA-B	2005 Apr 15	4.13	3.64	−20.27	0.099	p
4860.1	VLA-B	2005 Apr 15	1.21	1.07	−27.24	0.053	p
4860.1	VLA-C	2005 Aug 9	3.89	3.56	−25.00	0.059	p
4850.0	Green Bank 91m/GB6	1986–1987	222	194		5	8
8460.1	VLA-B	2005 Apr 15	0.71	0.64	−34.99	0.034	p
8460.1	VLA-C	2005 Aug 9	2.29	2.10	−50.32	0.041	p

References along with the names of some of the well-known surveys. (1) VLSSr: Lane, Cotton & van Velzen (2014); (2) 6C: Hales, Baldwin & Warner (1988); (3) MSRT: Zhang et al. (1997); (p) this paper; (4) WENSS: Rengelink et al. (1997); (5) B3: Ficarra, Grueff & Tomassetti (1985); (6) NVSS: Condon et al. (1998); (7) FIRST: Becker, White & Helfand (1995); (8) GB6: Gregory et al. (1996)

tified in Faint Images of the Radio Sky at Twenty-cm survey at 1400 MHz (FIRST; Becker, White & Helfand 1995). That list has been critically reviewed by Nandi & Saikia (2012) who confirmed the double-double nature of only 23 objects including J1706+4340. However, this study was begun in 2004, triggered by the work presented by Marecki et al. (2006) also related to restarted activity in AGNs but focused on the so-called core-dominated triple (CDT) sources. CDTs could be the early stages of DDRSs when the inner double is still too compact to be resolved in the maps encompassing the whole double-double structure.

Marecki et al. (2006) devised an automated procedure to select CDTs from FIRST. Each FIRST source with a flux density listed in that catalogue being greater than a particular threshold (75 mJy) was picked and then a pair of sources straddling it, i.e. the potential lobes, was sought within a 2-arcmin radius of the initially selected source – the potential core. It was required that the peak flux densities of the putative lobes were less than 30 per cent of that of the putative core. That threshold was somewhat arbitrary, but was based upon an initial, extensive visual inspection of FIRST maps: the peak flux densities of the lobes in the vast majority of sources with the required morphology fell well below that limit anyway.

Owing to the above selection procedure, it was possible to select many CDTs but it had one side effect that was not destructive to the CDT selection process and in the end turned out to be fortunate. If a potential CDT core was accompanied with another nearby compact source and if such a double shared a common pair of lobes, the algorithm formally detected two CDT candidates, each centred on one of the two point-like sources but sharing the same pair of the outer lobes. It follows that identifying such cases was equivalent to a selection of potential DDRSs. In order to make sure that those were indeed DDRSs, the positions of optical objects near the centre of the field were taken into account. Eventually, it was found

that in one such case neither of the two alleged CDT cores was an actual one but both straddled the optical/infrared object. Because of the presence of the common pair of large-scale lobes found by the algorithm, the whole selection process by Marecki et al. (2006) led to a serendipitous discovery of a new DDRS – J1706+4340 – in which the point-like sources appear as the inner pair of mini-lobes co-linear with the outer pair of extended but diffuse lobes.

3 OPTICAL AND INFRARED DATA

According to Sloan Digital Sky Survey (SDSS; Adelman-McCarthy et al. 2008), the position of the stellar-like object associated with J1706+4340 is RA=17^h06^m25^s.44, Dec.=+43°40′40″.16. Its SDSS optical magnitudes are: u=22.03±0.16, g=20.79±0.03, r=19.81±0.02, i=19.26±0.01, and z=18.79±0.03. Its photometric redshift based on the sixth SDSS release is z=0.525±0.051. This makes 1 arcsec on the sky to be an equivalent of 6.242 kpc.

The *Wide-field Infrared Survey Explorer* satellite (Wright et al. 2010) catalogue gives the following magnitudes of J170625.43+434040.1: W1(3.4 μ m)=14.676 ± 0.027, W2(4.6 μ m)=13.957 ± 0.031, W3(12 μ m)=11.415 ± 0.135, and W4(22 μ m)=8.557. According to Gürkan, Hardcastle & Jarvis (2014) and Wright et al. (2010), the calculated colours (W1-W2)=0.719 and (W2-W3)=2.542 indicate that the central source is of an AGN type and that the parent object is located close to the area occupied by quasars. Using the infrared photometric data given above as well as the Two Micron All-Sky Survey (Skrutskie et al. 2006) measurements, we fitted the spectral energy distribution (SED) of the parent object with the Code Investigating

Table 2. Flux densities of different components of J1706+4340

Frequency (MHz)	Total structure Observed	Flux density (mJy)			Outer structure	
		<----- Observed NE lobe	Inner structure Observed SW lobe	-----> Model fit NE+SW	Observed	Model fit
(1)	(2)	(3)	(4)	(5)	(6)	(7)
73.8	1419±380 ^a					
151.5	1170±110				708.8±110	692.0
152.2	1125±60				665.7±60	688.8
232.0	650±65 ^b				323.5±65	453.7
240.1	878±47				560.3±47	438.3
326.9	548±29				300.9±30	320.1
408.0	429±20 ^c				222.3±20	254.2
612.2	334±17	20.19±1.04	134.44±6.73	147.3	179.6±16	164.3
1400.0	148±8			78.2		
1400.0		9.02±0.72	70.66±3.59	78.2	68.2±7.5	60.8
1425.0		7.08±0.38	62.01±3.14	77.1		
1425.0		9.36±0.54	66.13±3.32	77.1		
4850.0	36.1±7.4				7.4±3.6	8.20
4860.1		3.27±0.21	25.03±1.30	27.6		
4860.1		3.26±0.20	25.85±1.27	27.6		
8460.1		2.05±0.13	15.04±0.76	16.8		
8460.1		2.23±0.14	16.28±0.87	16.8		

^aThe original flux density of the VLSSr survey (RBC scale; Roger, Bridle & Costain 1973) was multiplied by a factor of 0.9 to suit the Baars et al. (1977) scale;

^bthis is the peak flux and the error is 10 per cent of the flux;

^cthe original B3 flux density which is given in the CKL scale (Conway, Kellermann & Long 1998) is according to Baars et al. (1977) multiplied by a factor of 1.129 to the common Baars scale.

GALaxy Emission (CIGALE) package¹ (Roehlly et al. 2014). The SED is concordant with the SDSS magnitudes and the resultant photometric redshift is slightly smaller but – accounting for its uncertainty – still consistent with the SDSS estimate given above.

4 MULTIFREQUENCY RADIO OBSERVATIONS

For the purpose of this study, we analysed the data we acquired ourselves using the VLA and GMRT but also those available in the archives. Details of the observations are shown in Table 1 and in the three following subsections. The flux densities of different parts of the radio structure of J1706+4340 are listed in Table 2.

4.1 GMRT observations and data analysis

We performed dedicated observations of J1706+4340 with GMRT in three frequency bands: 152, 240, and 612 MHz, the latter two being obtained in dual frequency mode. The project code was 20_005 and the observations were carried out on 2011 August 25 and 31 for the 152 and 240/612 MHz bands, respectively. Data were recorded using 8-s integration time with the available frequency band divided into 256 channels. The usual scheme of observing phase calibrator interlaced with the observation of the target source was adopted. Flux density calibrators 3C286 and 3C48, respectively, were observed for about 15 min. at the beginning and at end of each observing run. Phase calibrators 3C309.1 and 3C286 were used at

frequencies centred at 152 and 240/612 MHz, respectively. The total integration time on the target source was about 5.3 and 5.5 h at 152 and 240/612 MHz, respectively.

Data reduction was carried out following standard calibration and reduction procedures in Astronomical Image Processing System (AIPS). Data were edited for strong radio frequency interference and then standard flux, phase, and bandpass calibrations were applied. The deconvolved images were made using the task IMAGR, where the field of view covering the primary beam was subdivided into a number of facets. Several rounds of phase-based self-calibration were performed. The resultant image was then corrected for the primary beam using the task PBCOR.

The flux density calibration errors are assumed to be 5 per cent at 612.2 and 8 per cent at 240.1 and at 152.2 MHz. The flux density measurements and their errors are shown in Table 2. The images at 152.2 and 612.2 MHz are shown in Fig. 1. The quality of the 240.1 MHz map is not satisfactory, therefore we do not present it here and use it only for the measurement of the total flux density of the source at this frequency.

4.2 VLA observations and data reduction

We observed J1706+4340 with the VLA at 1425 (conf. A and B), 4860 (conf. B and C), and 8460 MHz (conf. B and C) between 2005 April and 2006 February. The exact dates of these observations along with the beam sizes are shown in Table 1. They are marked with ‘VLA’ followed by the letter A, B, or C – it denotes the configuration – in column (2) of that table and the letter ‘p’ in column (6). The length of each observation is given in the caption of Fig. 2. 3C286 was used as an amplitude and J1707+4536

¹ CIGALE code is publicly available at <http://cigale.lam.fr>.

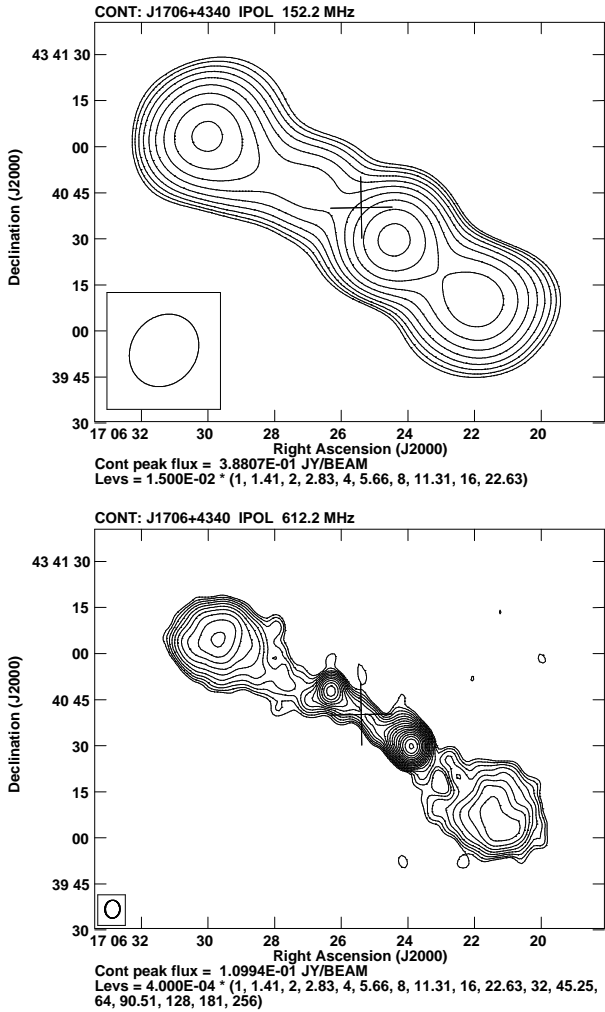


Figure 1. GMRT images. Upper panel: 152.2 MHz; Lower panel: 612.2 MHz. Crosses in each panel indicate the position of the parent optical object. The size of the beam is indicated by an ellipse in the bottom left corner of each panel.

as a phase calibrator. Data reduction was carried out in AIPS in a standard way. The flux density measurements and their errors are shown in Table 2. The images were generated by AIPS task IMAGR and are shown in Fig. 2.

4.3 Archival data

Apart from the dedicated observations itemized in subsections 4.1 and 4.2, we used publicly available images from the VLA Low-Frequency Sky Survey Redux at 74 MHz (VLSSr; Lane, Cotton & van Velzen 2014), the Westerbork Northern Sky Survey at 327 MHz (WENSS; Rengelink et al. 1997), FIRST, NRAO VLA Sky Survey at 1400 MHz (NVSS; Condon et al. 1998), and the Green Bank 4850 MHz northern-sky survey (GB6; Gregory et al. 1996). The flux densities obtained directly from the FITS maps (either produced for the purpose of this investigation or taken from the surveys) using AIPS tasks TVSTAT or JMFIT (in the case of point sources) are assumed to have the absolute flux calibration errors of 5 per cent. The flux densities taken from the literature are assumed to have the errors as determined in the corresponding references. In the case of the flux density values that

were not measured directly from the FITS maps (e.g. those of the extended structure) but estimated by other means, we propagate the errors of the directly measured flux densities. In the case of an extended source, a noise term related to the size of its structure (the product of map noise and square root of the number of beams per structure) was added, and the overall error is a root mean square of the calibration and noise errors. The resulting flux densities (along with the errors) of our target, given in the Baars et al. (1977) scale are listed in Table 2. In Fig. 3, we show the observational spectra of the whole source and of the inner north-eastern and south-western lobes. The spectra of the inner lobes are straight and flatter than the total source spectrum. Also, we obtained a combined spectrum of the inner lobes after adding the flux densities of both of them. Then we fitted a linear function to the data points in the form $\log[S(\text{mJy})] = (-0.81 \pm 0.02) \times \log[\nu(\text{MHz})] + (4.43 \pm 0.07)$. Finally, to obtain the flux densities of the outer lobes between 73 and 408 MHz, we subtracted the predicted flux density of the inner lobes from the spectrum of the whole source. The remaining values at 612, 1400, and 4850 MHz come from direct subtraction of the flux density figures of the inner structure from the flux density of the whole source.

4.4 Overall radio structure

The projected linear sizes of the inner and outer structures are 200 and 750 kpc, respectively. Based on the latter figure, J1706+4340 can be labelled a giant radio galaxy (GRG)². The 1400 MHz luminosity of the inner and outer structures is $\log(P_{\text{inn}}) = 25.88 \text{ W Hz}^{-1}$ and $\log(P_{\text{out}}) = 25.85 \text{ W Hz}^{-1}$, respectively. This is a rare case of a DDRS whose inner double is as luminous as the outer one. There is a characteristic brightness asymmetry in the lobes – whereas the north-eastern outer lobe is only a little brighter than its opposite counterpart, the inner south-western lobe is much more luminous than the north-eastern one (cf. the fluxes in columns (3) and (4) of Table 2). No hotspots are visible in the outer lobes. This is particularly well pronounced in the 1400 MHz VLA image (Fig. 2, upper-left panel). The spectra of the outer lobes are very steep above 1400 MHz, they are thus well imaged only with GMRT at 612.2 MHz (Fig. 1, lower panel); at this frequency the lobes are still strong while the resolution of the instrument is the highest. Only the 8460 MHz images reveal a very weak radio core at the position of the optical counterpart. Its flux density is below 0.4 mJy.

Among the six VLA images (Fig. 2), the outer lobes can only be seen in the one acquired owing to the conf. B 1400 MHz observation (upper-left panel). In the case of conf. A observation at the same frequency, the fraction of the ‘missing flux’ due to diffuseness of the structures of the outer lobes must be close to unity, so that they are absent in that image. This is also the ultimate proof that the hotspots are missing there, otherwise they should have appeared there anyway due to their compactness. Because of diffuseness of structures and steepness of spectra as well as lack of hotspots, the outer lobes are not visible in the VLA images at 4860 and 8460 MHz.

² The minimum span of a GRG is 1 Mpc but for $H_0 = 50 \text{ km s}^{-1} \text{ Mpc}^{-1}$. For H_0 adopted here, that lower limit should be downsized to 700 kpc.

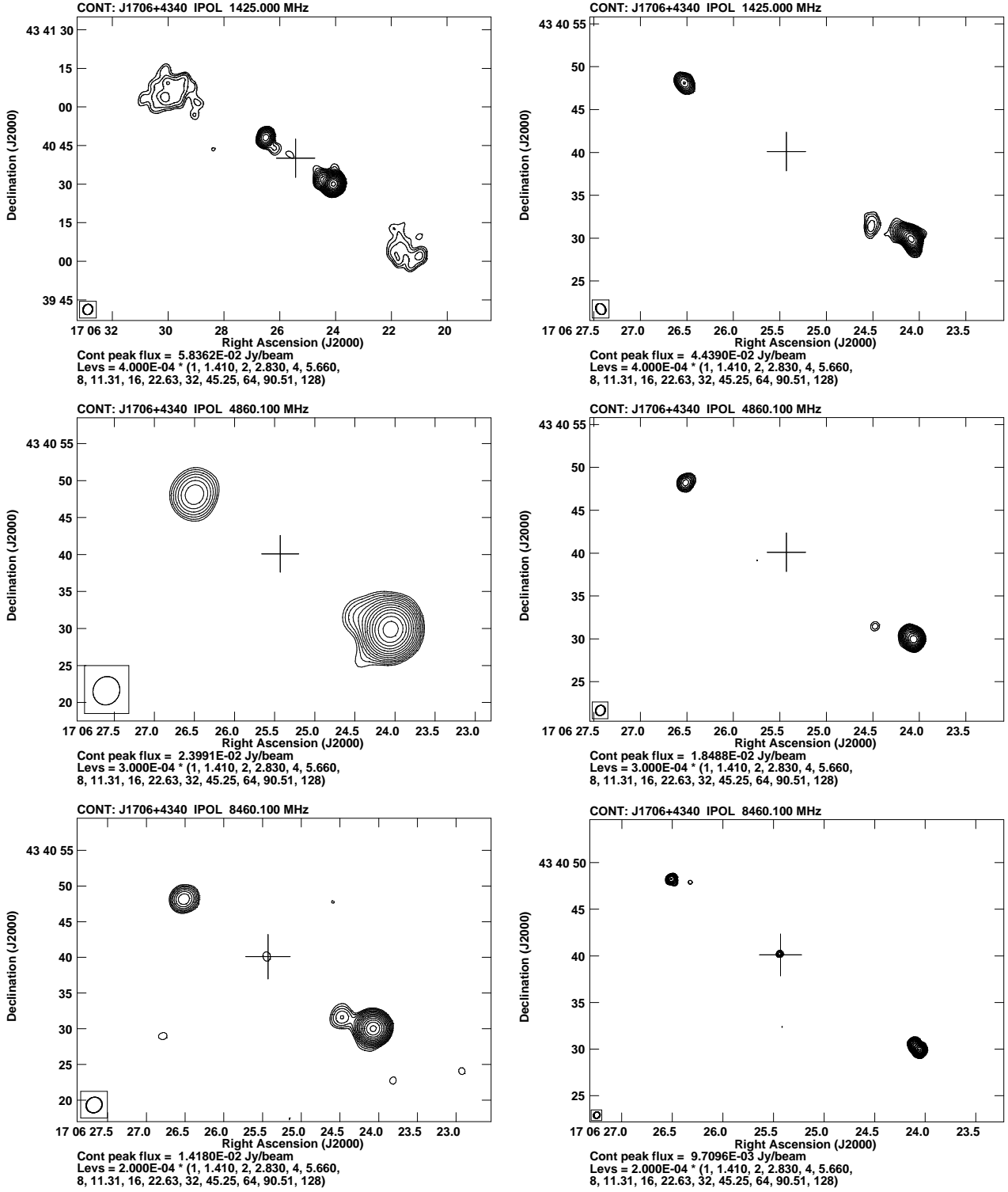
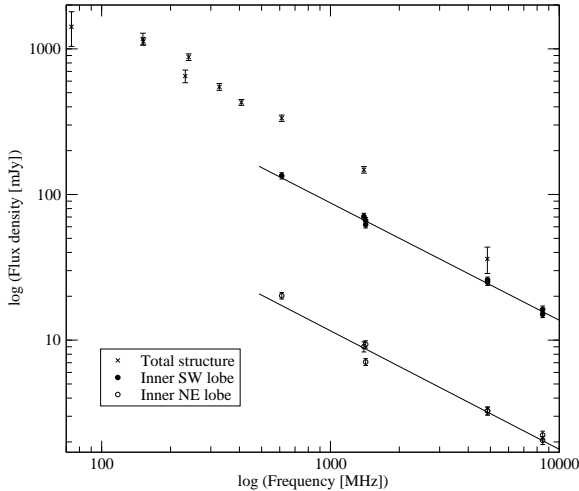


Figure 2. VLA images. Upper left: 1425 MHz, B-conf., integration time on source – 10^m50^s ; Upper right: 1425 MHz, A-conf., 9^m45^s on source; Middle left: 4860 MHz, C-conf., 9^m50^s on source; Middle right: 4860 MHz, B-conf., 18^m55^s on source; Lower left: 8460 MHz, C-conf., 31^m40^s on source; Lower right: 8460 MHz, B-conf., 28^m45^s on source. Upper left panel encompasses the whole source, other panels – only the inner lobes. Crosses in each panel indicate the position of the parent optical object. The size of the beam is indicated by an ellipse in the bottom left corner of each panel.

Table 3. Summary of the model parameters

Parameter (1)	Symbol (2)	Outer lobes (3)	Inner lobes (4)
Observed:			
Angular size of lobe ($\times 2$)	LAS	120 arcsec	32 arcsec
Length of lobe ($\times 2$)	D	749 kpc	200 kpc
Aspect ratio of lobe	R_T	2.15	10
Radio spectrum; i.e. monochromatic luminosity at a number of observing frequencies; $i = 1, 2, 3, \dots$	α_ν		
	$P_{\nu,i}$	Note(1)	Note(2)
Set:			
Adiabatic index of jet material	Γ_j	4/3	4/3
Adiabatic index of lobe material	Γ_ℓ	5/3	4/3
Adiabatic index of ambient medium	Γ_x	5/3	5/3
Adiabatic index of magnetic field	Γ_B	4/3	4/3
Minimum of initial electron Lorentz factor	γ_{\min}	1	1
Maximum of initial electron Lorentz factor	γ_{\max}	10^7	10^7
Core radius of ambient density distribution	a_0	2 kpc	–
Exponent of ambient density distribution	β	1.5	1.5, 0
Ratio of energy densities of thermal and relativistic electrons	k'	0, 1	0
Free:			
Jet power	$Q_j(W)$		
External density at core radius	$\rho_0(\text{kg m}^{-3})$		
Exponent of initial power-law energy distribution of relativistic electrons	p	$= 1 + 2\alpha_{\text{inj}}$	
Source (lobe) age	$t(\text{Myr})$		

Notes. (1) Relevant luminosities are calculated with flux densities shown in column (6) of Table 2. (2) Relevant luminosities are calculated with flux densities in columns (3)+(4) of Table 2.

**Figure 3.** Radio spectrum of the different parts of J1706+4340. Straight lines indicate power-law fit to the inner NE and SW lobes.

5 DYNAMICAL EVOLUTION ANALYSIS

5.1 Numerical code

Following the earlier work of Machalski, Jamrozy & Saikia (2009); Machalski, Jamrozy & Konar (2010) and Machalski (2011), the dynamical analysis presented in this study has been carried out using DYNAGE code (Machalski et al. 2007) based on the analytic model for the evolution of FR II-type radio sources. It combines the pure dynamical model of Kaiser & Alexander (1997)

with the model of expected radio emission from a source under the influence of the energy loss processes elaborated by Kaiser, Dennett-Thorpe & Alexander (1997) – the KDA model. For a given set of observables, this numerical code allows one to solve the inverse problem, i.e. to determine four free parameters of the KDA model: (1) the initial power-law energy distribution of the relativistic electrons p related to the effective injection spectral index α_{inj} (see Table 3), (2) the jet power Q_j , (3) the density of the external gaseous medium near the radio core ρ_0 , and (4) the age of the source's radio structure t .

A detailed description of how to apply the above code was given by Machalski, Jamrozy & Saikia (2009). Yet, it is worth mentioning here that determination of the values of these four parameters of the model is possible by a fit to the observational parameters of a source: its projected linear size D , the volume V , the radio power P_ν and the radio spectrum α_ν that provides $(P_\nu)_i$ at a number of observing frequencies $i = 1, 2, 3, \dots$. As in the KDA model, a cylindrical geometry of the source (its lobes) is assumed, $V = \pi D^3 / 16 R_T^2$, where R_T is their axial ratio. Similarly, the minimum-energy condition for the ratio of the energy density of the magnetic field in the lobes to that of all particles is enforced by setting $r = (1 + p) / [4(k' + 1)]$. This is justified by observations that the magnetized material in the lobes of FR II-type sources appears to be close to the minimum-energy conditions (cf. Croston et al. 2005; Kataoka & Stawarz 2005). The values of the remaining free parameters of the model have to be assumed. These are the following: the core radius a_0 , the exponent β describing the ambient density profile $\rho(d) = \rho_0(d/a_0)^{-\beta}$, the adiabatic indices in equations of state for the jet material, the magnetic field, the ambient medium, and the source (its lobes) as a whole, Γ_j , Γ_B , Γ_x and Γ_ℓ , respec-

Table 4. Model and derivative parameters for the inner and the outer structure (lobes) of J1706+4340

Parameters (1)	Inner structure		Outer structure	
	$\beta=1.5$ (2)	$\beta=0$ (3)	$k'=0$ (4)	$k'=1$ (5)
Model:				
α_{inj}	0.554	0.544	0.526	0.54
$Q_j (\times 10^{37} \text{ W})$	2.63	3.48	2.59	4.40
$\rho_0 (\times 10^{-22} \text{ kg m}^{-3})$	5.43	0.075	18.6	22.3
$t (\text{Myr})$	—	—	294	262
$t_j (\text{Myr})$	11.8	12.3	275	244
Derivative:				
$v_h/c (\times 10^{-3})$	23.7	15.9	2.86	3.20
$\rho_{(D/2)} (\times 10^{-24} \text{ kg m}^{-3})$	1.53	7.25	0.73	0.87
$p_t (\times 10^{-13} \text{ N m}^{-2})$	9.24	5.34	1.12	1.68
$B_t (\text{nT})$	1.75	1.32	0.45	0.42
$\chi^2_{\text{red.}}$	2.21	2.74	2.63	2.68

tively. The other free parameters to be assumed are the following: the Lorentz factors determining the energy range of the relativistic electrons used in integration of their power-law distribution $\gamma_{i,\text{min}}$ and $\gamma_{i,\text{max}}$, and the ratio of the energy density of thermal particles to that of the relativistic electrons k' .

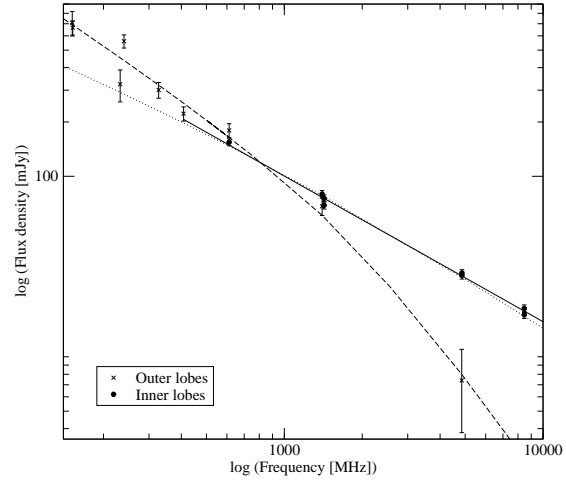
The original KDA model assumes a constant and uninterrupted jet flow delivering relativistic gas to the expanding lobes throughout the whole lifetime of a source. However, the radio maps in Figs 1 and 2 show no evidence for active hotspots in the outer lobes. This suggests that they are no longer supplied with energy by active jets. Taking into account the presence of the inner lobes' structure, we assume that the energy supply to the outer lobes ceased relatively recently in terms of the total age of the source. Therefore, in order to analyse evolution of this structure in the framework of the discussed scenario, we have to introduce one more free parameter of the model – the primary jet duration t_j .

5.2 Application of the model and fitting procedure

The analytical model described in Section 5.1 has been applied to the observational data of the inner and outer lobes of J1706+4340. The set of the model parameters with their values assumed for the given pair of lobes is shown in Table 3.

5.2.1 Inner lobes

As a first step, we apply the model to the observational data of the inner lobes because they are much better determined than those for the outer ones. Though the radio spectra for each of the inner lobes are derived, it should be pointed out that their unusually high asymmetry in the observed luminosity ($\sim 1:8$) poses a difficulty for the modelling. Indeed, such asymmetry induces significantly different values of the model parameters of individual lobes, like Q_j , ρ_0 , and t . In this context, some self-consistent model solutions explaining the case by different ambient density profiles along the opposite jets were proposed by Machalski, Jamroz & Saikia (2009) and Machalski (2011) but for the primary (outer) lobes in a sample of giant radio sources. A similar issue related to the secondary (inner) lobes of a known DDRS J1548–3216 was discussed by Machalski, Jamroz & Konar (2010), however in that case the

**Figure 4.** Fitted spectra to the lobes. Straight line – power-law fit to the inner lobes. Dotted curve – DYNAGE fit to the inner lobes. Dashed curve – DYNAGE fit to the outer lobes.

relevant asymmetry was only about 1:2. The same aspect in two other DDRSs – B1430+333 and B1843+620 – was analysed and discussed by Brocksopp et al. (2011). Here, we confine our analysis to the whole inner structure, i.e. omitting differences between the opposite lobes and using one half of the sum of the flux densities in columns (3) and (4) of Table 2 to calculate the radio luminosities at a given observing frequency.

It has been pointed out by e.g. Kaiser & Cotter (2002), Brocksopp et al. (2007), Brocksopp et al. (2011), Machalski et al. (2007), and Machalski, Jamroz & Konar (2010) that due to a large number of free parameters, the applied analytical model is very flexible hence quite different sets of its parameters may fit the observational data – especially the radio spectrum – with a comparable level of significance. Since an independent observational constraint on the model parameters, e.g. on the ambient medium density provided by the X-ray measurements, is not available here, particularly for a density inside the outer lobes of J1706+4340, searching for a minimum of the jet energy delivered into the source, $(Q_j \times t_j)_{\text{min}}$ is included into our procedure.

We investigate two opposing models. In the first one, a power-law density distribution of the external gaseous medium with a standard exponent $\beta = 1.5$ is assumed, while in the other one it is assumed that the inner lobes evolve into a pure uniform medium with $\beta = 0$ inside a cocoon formed and inflated by the material of the primary jet flow. In both models, we assume that the lobes are filled only with magnetic fields and relativistic particles governed by a relativistic equation of state with $\Gamma_\ell = 4/3$. Columns (2) and (3) of Table 4 show the fitting results for these two models, respectively. The relevant flux densities resulting from the first model are shown in column (5) of Table 2 for a comparison with observations and Fig. 4 shows the model spectrum compared to the observed data points. The differences between various physical parameters resulting from these two models are further discussed in Sections 6.3 and 6.4.

5.2.2 Outer lobes

Contrary to the inner structure, the energy density of the outer hence older lobes may contain some contribution from thermal non-radiating particles, i.e. $k' \neq 0$. We thus set $\Gamma_\ell = 5/3$ for these

lobes. Note that when the jet activity is terminated, the adiabatic expansion of the primary lobes is expected to slow down and faster energy losses of the relativistic electrons are presumed. Therefore, two different phases of their dynamical evolution should be considered, the first one corresponding to the ongoing feeding of the lobes by the active jets (source ages $t \leq t_j$) and the second one corresponding to the case when the jet flow has ceased (ages $t > t_j$). Importantly, the evaluation of the fading lobes' luminosities is done taking into account only those relativistic electrons that were injected into the lobes during the first phase of evolution, i.e. the ongoing jet activity. The integration over the injection time for the expected radio emission is performed following the prescription given by Kaiser & Cotter (2002) for relic radio sources.

As a first step, we search for the best model solution with $k' = 0$. The fitted values of the model parameters are shown in column (4) of Table 4. Note that the resultant values of α_{inj} are almost identical in the best solutions for both the inner and outer lobes. This is in an agreement with the main conclusion drawn by Konar & Hardcastle (2013) based on a study of a sample of eight DDRSs (J1706+4340 was not included there). Moreover, the values of α_{inj} and Q_j we obtained follow the correlation between α_{inj} and Q_j found by Konar & Hardcastle – see the bottom panel of their fig. 2 – even though the method of determination of α_{inj} and Q_j they used and the one we adopted here were different. Those different approaches and their implications for the α_{inj} and Q_j estimates are further discussed and commented in Section 6.2.

It should also be noted that the derived jet power during its primary activity is comparable to its fitted value during the recurrent activity. The above result, obtained with the fitting procedure carried out independently for the outer and inner structures, may indicate that Q_j cannot vary significantly between the two active phases. However, the model of the inner lobes with $\beta = 0$ admits slightly higher value of Q_j than that for the outer lobes. It is obvious that a contribution to the energy density of these lobes from possible thermal particles requires an increase of the jet power to explain their observed radio emission. Therefore, we investigate another model for the outer lobes with $k' > 0$, finding that $k' = 1$ already satisfied a condition $Q_{j,\text{out}} \geq Q_{j,\text{inn}}$. The relevant model parameters are shown in column (5) of Table 4 and the flux densities resulting from the model with $k' = 0$ – in column (7) of Table 2.

Except for the fitted values of the model parameters defined in Section 5.1, some derivative physical parameters of the radio structures are also shown in Table 4. These are the following: the longitudinal expansion velocity of the lobe given by differentiation of the formula for the jet length (cf. equations (4) and (5) in Kaiser & Alexander 1997), the ambient density at the end of the lobe, $\rho(D/2)$, the pressure inside the lobe, $p_\ell \equiv p_\ell(t_j)$ and $p_\ell(t) = p_\ell(t_j)(t/t_j)^{-c_1}$ for the inner and the outer lobes, respectively, where $p_\ell(t_j)$ corresponds to the cocoon's pressure given by equation 20 in Kaiser & Alexander (1997) and $c_1 = 6(\Gamma_\ell - 1)/(7 + 3\Gamma_\ell - 2\beta)$ (cf. Kaiser & Cotter 2002), and a mean value of the magnetic field strength, $B_\ell = (2\mu_0 u_B)^{1/2}$, where $u_B = (p_\ell \times r)/[(\Gamma_\ell - 1)(r + 1)]$ is the magnetic field energy density.

Note that all the models reveal a similar agreement with the observational data. The last line in Table 4 presents the χ^2 values reduced by the degree of freedom. Although these values are rather high, they are overestimated by the large discrepancy between the flux densities measured on the Miyun Synthesis Radio Telescope (MSRT) and GMRT maps at ~ 240 MHz used to determine the radio spectrum of the outer lobes (cf. Fig. 4), as well as likely underestimated flux density at 1425 MHz measured in the VLA A-conf. image in the spectrum of the inner lobes.

6 DISCUSSION

6.1 Uncertain redshift

Since the spectroscopic redshift of the host galaxy of J1706+4340 is not available, we use its photometric estimate – it has been given in Section 3. It is among the highest redshift values of radio galaxies suspected for a recurrent nuclear activity (cf. Nandi & Saikia 2012). Note that only B1843+620 galaxy ($z = 0.519$) belongs to the group of well-studied DDRSs at redshift of ~ 0.5 . Therefore, the dynamical model parameters of J1706+4340 derived by the fit to its observational data, i.e. the energetics, ages, etc., can be less certain than those for sources with spectroscopic redshift available, and hence with more certain distance to the observer enabling a better determination of their size, luminosity, and radio spectrum. Taking into account possible overestimation of the adopted redshift, we performed the fitting procedure for the inner and the outer lobes adopting $z = 0.3$. Such hypothetical much lower value of redshift enables an investigation of its influence on the fitted values of α_{inj} and Q_j . Note that at this redshift both pairs of the lobes will appear less luminous and their span shorter compared to the respective values at $z = 0.525$. In particular, the span of the inner/outer lobes will be ~ 140 kpc and ~ 530 kpc, respectively, placing J1706+4340 below the lower limit of the size of a GRG mentioned in Section 4.4. Likewise a decreased luminosity will imply a lower jet power adequate to provide the observed radio emission. Indeed, we found the best-fitting solution with $\alpha_{\text{inj}} = 0.539$, $Q_j = 0.84 \times 10^{37}$ W and $t = 15.8$ Myr for the inner lobes modelled with $\beta = 0$, as well as $\alpha_{\text{inj}} = 0.530$, $Q_j = 0.92 \times 10^{37}$ W, $t = 340$ Myr and $t - t_j = 28$ Myr for the outer lobes assuming $k' = 1$. As expected, the best-fitting values of α_{inj} and, especially, of Q_j diminish with decreasing redshift, thus being compatible with the $\alpha_{\text{inj}} - Q_j$ correlation noticed and discussed by Konar & Hardcastle (2013).

6.2 Remarks on the 'spectral index–jet power' correlation and their values during consecutive episodes of activity

As noted in Section 5.2.2, our results obtained from the dynamical analysis follow the $\alpha_{\text{inj}} - Q_j$ correlation determined in a different way. Konar & Hardcastle (2013) used the synchrotron JP model (Jaffe & Perola 1973) to fit the value of α_{inj} and a frequency break ν_{brJP} in radio spectra of the sources in their sample that allow determination of the spectral age of actually radiating relativistic electrons τ_{syn} . In order to estimate the value of Q_j , they applied the relation equating the total energy deposited by the jet inside the volume of the lobe V_ℓ , $(\Gamma_\ell - 1) Q_j t_j \approx p_\ell V_\ell$, admittedly identifying t_j with τ_{syn} . Their approach results in a steep slope of the investigated correlation. In fact, that slope flattens due to evidently higher jet powers if α_{inj} and Q_j values are determined from the dynamical analysis. For example, Machalski, Jamroz & Saikia (2009) have already modelled most of the sources from the sample of Konar & Hardcastle providing a comparison between spectral and dynamical α_{inj} values, and finding Q_j values $\sim (1.2-2)$ times higher than those in Konar & Hardcastle. The latter result is easily explained by the fact that their approach accounts for the synchrotron losses only but not for the adiabatic expansion of the lobes.

However, it is worth emphasizing that Konar & Hardcastle (2013) have analysed and discussed an interesting problem of whether the injection spectral index and the jet power in the outer and the inner lobes of DDRSs are expected to differ or not. They pointed out that the principal factor determining α_{inj} should be the strength of the jet-termination shock which, in turn, should depend

on the external medium density ρ_x . Since the inner lobes are immersed in the cocoon material of the outer lobes whose ρ_x is very likely different from the density of the primary environment surrounding the latter ones, one can expect a systematic difference between $\alpha_{\text{inj,inn}}$ and $\alpha_{\text{inj,out}}$, which is not observed. On the other hand, there is commonly expected that Q_j depends on the supermassive black hole (SMBH) mass, the accretion disc properties and accretion rate, and perhaps the SMBH spin (e.g. Blandford & Znajek 1977, Tchekhovskoy et al. 2010). The question why a correlation between the spectral index and the jet power – the quantities that are ruled by quite different physical conditions inside the nucleus of a host galaxy and in the external environment – exists, deserves further study.

6.3 Age and intermittent activity

The age solutions for the inner and outer lobes collected in Table 4 suggest that the last renewal of the jet activity took place about 12 Myr ago, thus its present age is about 4–5 per cent of the age estimated for the outer lobes' structure. On the other hand, the quiescent period time emerging from the model fits, $t - t_j$, of about 18–19 Myr is not much larger than the age determined for the inner structure. However, it should be increased by the real time elapsed between the last jet material ejected by the AGN and the time it reached the head of the still-expanding lobe which is not taken into account in DYNAGE algorithm. When this is accounted for, the age proportions are very similar to those found in other already investigated DDRSs.

The first attempt to estimate the time-scales of the interruption of the jet flow was undertaken by Kaiser, Schoenmakers & Röttgering (2000). They showed that this 'elapsed' time is comparable to the age of inner lobes in their sample of five very large DDRSs including B1450+333 and B1834+620 further modelled by Brockopp et al. (2011) in terms of their dynamical evolution. Also, Kaiser, Schoenmakers & Röttgering (2000) found comparable values for the ages of the inner lobes and the time lag $t - t_j$, especially in the case of B1834+620. Another example of intensively studied DDRS is PKS B1545–321 (J1548–3216). Its restarted jet activity was analysed and discussed by Saripalli, Subrahmanyan & Udaya Shankar (2003), Safouris et al. (2008), and Machalski, Jamroz & Konar (2010). The inner lobes are deeply immersed into the extended cocoon of the primary radio emission implying a very short time-scale between cessation and renewal of the jet activity estimated as (0.5–1) Myr, while the fitted age of these lobes is $\sim (5-9)$ Myr.

Duration of the quiescent phase can be also estimated from the curvature of the radio spectrum due to the energy losses caused by the synchrotron and inverse-Compton processes. In order to compare such estimate with that derived using DYNAGE, the spectral JP model has been fitted to the spectrum of the outer lobes of J1706+4340, and the value of $\nu_{\text{BJP}} = 1.8^{+40}_{-0.3}$ GHz has been determined using SYNAGE package (Murgia 1996) adopting the injection spectral index $\alpha_{\text{inj}} = 0.54$, and the magnetic field strength $B_\ell = 0.42$ nT, i.e. the values found using DYNAGE. It follows that duration of the period of quiescence is 27^{+2}_{-22} Myr. As can be seen, the uncertainty of this period is very unsymmetrical; its upper limit is a little higher than (18–19) Myr estimated with the dynamical analysis, however rather expected as discussed above.

6.4 Subsonic/supersonic expansion

Not only lacks J1706+4340 optical spectrum but there are also no X-ray observations available that, in principle, could provide some constraints on the model parameters including density, pressure, and kinetic temperature of the intergalactic medium surrounding the DDRS under investigation. Nevertheless, a crude estimates of the ambient kinetic temperature and the sound speed in the ambient gaseous environment are possible using the derivative physical parameters shown in Table 4. From the equation of state (for a perfect gas):

$$kT = \mu m_H p / \rho \sim \mu m_H p_h / \rho_{(D/2)} \quad \text{and}$$

$$c_s = [(\Gamma_x kT) / (\mu m_H)]^{1/2},$$

where the pressure of the jet's head (working surface of the bow shock) is taken as $p_h = \mathcal{P}_{\text{hl}} p_\ell$, and the ratio \mathcal{P}_{hl} is adopted from Kaiser (2000). Assuming the mean atomic weight $\mu = 0.62$, we find $kT = 4.9$ keV and $c_s = 0.00374c$ for the outer lobes. Since the model with $k' = 0$ gives $v_h/c = 0.00286c$, the ratio $v_h/c_s = 0.77$ supports a presumption based on a lack of hot spots and any trace of a bow shock on the radio maps, that the longitudinal expansion of these lobes is subsonic, i.e. the Mach number < 1 . It is worth noting that the above ambient temperature is fully compatible with the X-ray temperatures in the samples of 20 powerful 3CR radio source (Belsole et al. 2007), and 31 nearby clusters of galaxies (Croston et al. 2008b), fitted to the observed counts made with the *XMM-Newton* and *Chandra* observatories.

Estimation of the kinetic temperature inside the cocoon surrounding the inner lobes is problematic because their gaseous environment is likely modified by the jet flow during the earlier phase of activity. Thus, using the more conservative value of p_ℓ instead of p_h in calculation of kT values from the two models investigated in Section 5.2.1 for these lobes, we find $kT = 3.9$ keV, and $c_s = 0.0030c$ in the model with $\beta = 1.5$, as well as $kT = 0.5$ keV and $c_s = 0.0011c$ in the model with $\beta = 0$. So, dividing the corresponding values of the advance speed of the inner lobes v_h/c (inserted in Table 4) by the relevant sound speeds given above, we find the Mach number in the range 8–15. The value $kT < 1$ keV estimated in the frame of the model with $\beta = 0$ perhaps permits to distinguish the model with the uniform external density distribution, because such temperatures were found in the centres of haloes or clouds of X-ray emitting gas surrounding nearby radio galaxies (cf. Allen et al. 2006; Lanz et al. 2015). Also the kT value, higher for the outer lobes than that for the inner ones, is in line with the electron density and temperature profiles presented in Croston et al. (2008a,b).

7 SUMMARY AND CONCLUSIONS

(i) In this article, we present a comprehensive study of a newly discovered DDRS J1706+4340. We carried out radio observations of this object with GMRT and the VLA at several frequencies ranging from 152 to 8460 MHz and we present images resulting from these observations. The double-double structure is clearly visible in these images albeit only at frequencies lower than or equal to 1425 MHz. The outer lobes are diffuse and show no traces of hotspots. It follows that they are in the coasting i.e. the final stage of their evolution.

(ii) We supplemented our data with those in the literature and constructed spectra of different parts of J1706+4340 covering more than two orders of magnitude wide frequency range:

from 74 to 8460 MHz. We modelled these spectra with `DYNAGE` code and determined the ages of both the outer and inner lobes, as well as duration of the quiescent period. The resulting age of the outer lobes (260 – 300 Myr) appears to be the oldest among relevant age estimates in other well-studied DDRSs, e.g. J0041+3224 (Saikia, Konar & Kulkarni 2006; Machalski 2011), B0925+420 (Kaiser, Schoenmakers & Röttgering 2000; Brocksopp et al. 2007), and those cited in Section 6.3 where, unlike in J1706+4340, the majority of them still reveal either weak hotspots or a trace of bow shocks.

(iii) The frequency break, ν_{br} , determined from the fit of the JP model to the outer lobes' spectrum with `SYNAGE`, together with the magnetic field strength, B_ℓ , found with `DYNAGE`, provide independent estimate of the quiescence period, fully compatible with that determined in the dynamical analysis. It is an order of magnitude shorter than the age of the outer lobes, whereas the age of the inner lobes is only 4–5 per cent of the outer ones. All these results fit the well established paradigm ruling the DDRSs: they are restarted sources where the two pairs of lobes are pertinent to two consecutive episodes of activity separated by a period of quiescence. Because of the appreciable steepness of the spectra of the outer lobes above ν_{br} , combined with their diffuseness, their apparent absence in the VLA images at 4860 and 8460 MHz may be considered explained.

(iv) The highly co-linear axes of both pairs of the lobes imply that the SMBH in the central AGN has a stable orientation. For the lack of noticeable distortions in the overall radio structure of J1706+4340, it is the spin of SMBH rather than e.g. an instability of the accretion disc that is likely to be responsible for the jet production. Therefore, it may be expected that the new jets, formed after disruption of their primary flow, should have the same power as the old jets. It is worth emphasizing that the above condition was almost fulfilled in `DYNAGE` solution shown in column (4) of Table 4. However, we show that an admixture of non-radiating particles in the older outer lobes, parametrized by $k' = 1$, increases the energy requirement providing satisfactory surplus of the jet power.

(v) We show how the pressure conditions in the lobes derived from `DYNAGE` solutions allow a crude estimation of the kinetic temperatures of the gaseous environment surrounding the outer and the inner lobes as well as the relevant speeds of sound. We note that the temperature estimate around the outer lobes is fully compatible with the X-ray temperatures measured in the samples of powerful 3CR radio sources and nearby clusters of galaxies. We also find that the current longitudinal (very likely adiabatic) expansion of the outer lobes is already subsonic, thus compatible with presumption that they are in the coasting stage of their evolution.

On the other hand, the head expansion of the inner lobes is an order of magnitude faster than the outer ones, and the relevant Mach number is around 10. Therefore, we conclude that these young lobes can substantially modify the surrounding matter by driving strong shocks and heating gaseous content of the old cocoon.

(vi) The extreme different values for the exponent of the external density distribution along the inner lobes assumed in the fitting procedure with `DYNAGE` though providing comparable ages and other model parameters (except of ρ_0), imply clearly different kinetic temperatures of the ambient medium, $kT > 1$ keV in the model with $\beta = 1.5$ and $kT < 1$ keV in that with $\beta = 0$. It seems that the latter solution is preferred because such temperatures are typical for the X-ray emitting haloes detected around nearby radio galaxies.

8 ACKNOWLEDGEMENTS

We warmly thank A. Kurcz for performing the SED fitting with `CIGALE`, as well as the referee for useful suggestions helping to improve the paper. We acknowledge the access to `SYNAGE` package provided by Dr Matteo Murgia. We thank the staff of GMRT that made these observations possible. GMRT is run by the National Centre for Radio Astrophysics of the Tata Institute of Fundamental Research. The National Radio Astronomy Observatory running the VLA is a facility of the National Science Foundation operated under cooperative agreement by Associated Universities, Inc. MJ and JM were supported by Polish NSC grant DEC-2013/09/B/ST9/00599.

REFERENCES

- Adelman-McCarthy J. K. et al. 2008, *ApJS*, 175, 297
- Allen S. W., Dunn R. J. H., Fabian A. C., Taylor G. B., Reynolds C. S., 2006, *MNRAS*, 372, 21
- Baars J. W. M., Genzel R., Pauliny-Toth I. I. K., Witzel A., 1977, *A&A*, 61, 99
- Becker R. H., White R. L., Helfand D. J., 1995, *ApJ*, 450, 559
- Belsole E., Worrall D. M., Hardcastle M. J., Croston J. H., 2007, *MNRAS*, 381, 1109
- Blandford, R. D., Znajek, R. L., 1977, *MNRAS*, 179, 433
- Brocksopp C., Kaiser C. R., Schoenmakers A. P., de Bruyn A. G., 2007, *MNRAS*, 382, 1019
- Brocksopp C., Kaiser C. R., Schoenmakers A. P., de Bruyn A. G., 2011, *MNRAS*, 410, 484
- Condon J. J., Cotton W. D., Greisen E. W., Yin Q. F., Perley R. A., Taylor G. B., Broderick J. J., 1998, *AJ*, 115, 1693
- Conway R. G., Kellermann K. I., Long R. J., 1963, *MNRAS*, 125, 261
- Croston J. H., Hardcastle M. J., Harris D. E., Belsole E., Birkinshaw M., Worrall D. M., 2005, *ApJ*, 626, 733
- Croston J. H., Hardcastle M. J., Birkinshaw M., Worrall D. M., Laing R. A., 2008a, *MNRAS*, 386, 1709
- Croston J. H. et al., 2008b, *A&A*, 487, 431
- Ficarra A., Grueff G., Tomassetti G., 1985, *A&AS*, 59, 255
- Gregory P. C., Scott W. K., Douglas K., Condon J. J., 1996, *ApJS*, 103, 427
- Gürkan G., Hardcastle M. J., Jarvis M. J., 2014, *MNRAS*, 438, 1149
- Hales S. E. G., Baldwin J. E., Warner P. J., 1988, *MNRAS*, 234, 919
- Jaffe W. J., Perola G. C., 1973, *A&A*, 26, 423
- Kaiser C. R., 2000, *A&A*, 362, 447
- Kaiser C. R., Alexander P., 1997, *MNRAS*, 286, 215
- Kaiser C. R., Cotter G., 2002, *MNRAS*, 336, 649
- Kaiser C. R., Schoenmakers A. P., Röttgering H. J. A., 2000, *MNRAS*, 315, 381
- Kaiser C. R., Dennett-Thorpe J., Alexander P., 1997, *MNRAS*, 292, 723
- Kataoka J., Stawarz L., 2005, *ApJ*, 622, 797
- Komissarov S. S., Gubanov A. G., 1994, *A&A*, 285, 27
- Konar C., Saikia D. J., Jamrozy M., Machalski J. 2006, *MNRAS*, 372, 693
- Konar C., Hardcastle M. J., 2013, *MNRAS*, 436, 1595
- Lane W. M. Cotton W. D., van Velzen S., Clarke T. E., Kassim N. E., Helmboldt J. F., Lazio T. J. W., Cohen A. S., 2014, *MNRAS*, 440, 327

- Lanz L., Ogle P. M., Evans D., Appleton P. N., Guillard P., Emonts B., 2015, *ApJ*, 801, 17
- Machalski J., 2011, *MNRAS*, 413, 2429
- Machalski J., Chyży K. T., Stawarz L., Koziel D., 2007, *A&A*, 462, 43
- Machalski J., Jamrozy M., Konar C., 2010, *A&A*, 510, A84
- Machalski J., Jamrozy M., Saikia D. J., 2009, *MNRAS*, 395, 812
- Marecki A., Thomasson P., Mack K.-H., Kunert-Bajraszewska M., 2006, *A&A*, 448, 479
- Murgia M., 1996, Laurea Thesis, Univ. Bologna
- Nandi S., Saikia D. J., 2012, *Bull. Astron. Soc. India*, 40, 121
- Proctor D. D., 2011, *ApJS*, 194, 31
- Rengelink R. B., Tang Y., de Bruyn A. G., Miley G. K., Bremer M. N., Roettgering H. J. A., Bremer M. A. R., 1997, *A&AS*, 124, 259
- Roehlly, Y., Burgarella, D., Buat, V., Boquien M., Ciesla L., Heinis S., 2014, in Manset N., Forshay P., eds, *ASP Conf. Ser.*, Vol. 485, *Astronomical Data Analysis Software and Systems XXIII*. Astron. Soc. Pac., San Francisco, p. 347
- Roger R. S., Bridle A. H., Costain C. H., 1973, *AJ*, 78, 1030
- Safouris V., Subrahmanyam R., Bicknell G. V., Saripalli L., 2008, *MNRAS*, 385, 2117
- Saikia D. J., Konar C., Kulkarni V. K., 2006, *MNRAS*, 366, 1391
- Saikia D. J., Jamrozy M., 2009, *Bull. Astron. Soc. India*, 37, 63
- Saripalli L., Subrahmanyam R., Udaya Shankar N., 2003, *ApJ*, 590, 181
- Skrutskie, M. F. et al., 2006, *AJ*, 131, 1163
- Spergel D. N. et al., 2003, *ApJS*, 148, 175
- Tchekhovskoy, A., Narayan, R., McKinley, J. C., 2010, *ApJ*, 711, 50
- Wright E. L. et al., 2010, *AJ*, 140, 1868
- Zhang X., Zheng Y., Chen H., Wang S., Cao A., Peng B., Nan R., 1997, *A&AS*, 121, 59